Particle Mixing in Rotating Fluidized Beds: Inferences about the Fluidized State

Gui-Hua Qian, István Bágyi, Robert Pfeffer, and Henry Shaw
Dept. of Chemical Engineering, Chemistry and Environmental Science, New Jersey Institute of Technology, Newark, NJ 07012

John G. Stevens
Dept. of Mathematical Sciences, Montclair State University, Montclair, NJ 07043

Particle motion in a rotating fluidized bed was studied by observing the mixing of two layers of particles of different colors. The particles in the two layers were either nearly identical, except for their color, or were of different density and size distribution. All of the particles were in the Geldart-A classification for conventional fluidized beds. After fluidization, but before mixing, the bed exhibited some fluid-like behavior, that is, the inner surface became radially uniform. For particle layers of the same material, mixing occurred after U_{mfc} was reached, with bubbles observed at the mixing velocity. No experimental difference between U_{mb} and U_{mfc} could be discerned; they either coincided or were nearly equal. Bubbles appeared to be responsible for particle motion and mixing. When the denser particles are placed on the distributor, the mixing behavior was similar to that observed for layers of the same material. However, when the less dense particles are placed on the distributor, mixing is dominated by differences in density and occurs before bubbles are visible.

Introduction

Although much basic and applied data on fluidization have been generated during the past 50 years (Davidson et al., 1985), some fundamental questions still need to be addressed. For example, Jackson (1998) concluded that a combination of careful bed height, fluid pressure drop, and fluctuation velocity measurements in beds of several diameters should be capable of providing a substantial amount of information about the particle phase stresses. Recently, Menon and Durian (1997) measured particle motions or local particle fluctuation velocities by diffusing-wave spectroscopy (DWS) in a conventional gas-fluidized bed of glass beads and demonstrated that the motion of macroscopic bubbles is the source of particle motions in the bed. They concluded that the homogeneous state of the bed known as the uniformly fluidized state (after incipient fluidization has occurred, but before bubbles are observed) is actually a weak solid in which particles are at rest. In the bubbling state, particles are carried in convection patterns with a downflow at the walls and an upflow in the middle of the bed. Superimposed on this overall convection is motion in the vicinity of rising bubbles, where particles are swept up with the bubbles.

Using DWS, Menon and Durian (1997) measured the mean-squared particle fluctuation velocity or granular temperature near the wall of their fluidized bed as a function of particle diameter and gas-flow rate. Similar experiments were done by Cody and coworkers (1996, 1997) by measuring the acoustic shot noise (ASN) excitation of the surface of the fluidized-bed vessel by random particle impacts. The results of all of these experiments are compared in a recent article by Cody et al. (1998), who show that for Geldart-B (Geldart, 1986) glass spheres ($d_p \geq 150$ μm), the agreement between the two independent sets of data is excellent, but, for Geldart-A glass spheres ($d_p \leq 120$ μm), there is a systematic difference between the two measurements. The DWS measurements of Menon and Durian (1997) do not show the bifurcation in the fluctuation velocity observed in the ASN measurements of Cody and coworkers (1996, 1997) below the Geldart B/A transition at $d_p \sim 120$ μm. The authors (Cody et al., 1998) attribute this difference to the fact that the experiments by Cody et al. were performed in a cylindrical vessel,

Correspondence concerning this article should be addressed to R. Pfeffer.

whereas those of Menon and Durian were performed in a square vessel together with the hypothesis that Geldart-A fluidization is dependent on particle circulation within the fluidized bed. To prove this point, they present theoretical arguments that the Geldart-A glass spheres of Menon and Durian are behaving like Geldart-B glass spheres due to the low shear circulation at the face of the square vessel. This hypothesis that Geldart-A fluidization is dependent on circulation within the fluidized bed, if correct, has significant implications for all experimental and theoretical research in the area of fluidization.

In a conventional fluidized bed, it is difficult to avoid circulation of the particles because of wall effects. Also, the minimum fluidization velocity is relatively low so that the range between the minimum fluidization and the minimum bubbling velocity is narrow even for Geldart-A particles. A rotating fluidized bed (RFB), on the other hand, has several advantages for these kinds of studies. There are negligible wall effects since the distributor comprises the cylindrical vessel, and the only ''walls'' are the end plates. Minimum fluidization velocities are also typically much higher than for conventional fluidized beds with initial fluidization occurring at the inner surface and proceeding rapidly outward with increasing gas velocity (Kao et al., 1987). However, it must be emphasized that there are essential differences between conventional fluidized beds and rotating fluidized beds. An important difference is the magnitude of the respective acceleration fields experienced by the bed particles. Thus, our results may not shed direct light on the discrepancy between the findings of Menon and Durian (1987) and Cody et al. (1996).

In this article, experimental results of mixing caused by Geldart-A particle motions in an RFB are presented. The simple experimental procedure is to load two different colored layers of particles consisting of the same or different materials. If the two colored layers of particles mix together, it is obvious that the particles have moved. At the same time, the relationship between pressure drop of the bed and superficial gas velocity is measured in the packed, partially fluidized, and totally fluidized-bed operating regions. Bed expansion was not measured, since in the rotating fluidized bed experiments, the bed is very shallow (approximately 1 cm) and is also nonuniform both radially and axially. By comparing observations of particle mixing and bubble formation with pressure drop, the point at which particle motion occurs can be determined. Kroger et al. (1980) have previously studied particle mixing in a centrifugal fluidized bed. Their visual observations show that bubbles are the primary mechanism causing radial mixing for Geldart-B and Geldart-D particles. Fluidization with bubbling at the freeboard surface was observed at the value of the predicted minimum fluidization velocity. However, Kroger et al. (1980) did not study mixing of Geldart-A particles.

The primary purpose of this article is to study motion and mixing as gas-flow rate increases. Therefore, no data are presented on the fluidization/defluidization hysteresis effect. This phenomenon was previously studied and reported in Qian et al. (1998). Pressure drop across a bed of alumina powder from the same batch used in the current experiments was measured with increasing and then decreasing gas-flow rate using the same experimental arrangement and conditions as reported in this article. Our results in Qian et al. (1998) show there is a slight difference between the pressure drop curves obtained with the increasing and decreasing gas-flow rate. These results are in good agreement with those of Tsinontides and Jackson (1993) for cracking catalyst (75 μm, mass mean diameter), who also established that the hysteresis effect is inversely related to the flowability of the particles. Studies of the hysteresis effect with glass beads (again, similar to those used in this article) show that no substantial pressure drop difference occurs with fluidization or defluidization. These results are in good agreement with the results of Cody et al. (1996) for glass beads in the Geldart-A region.

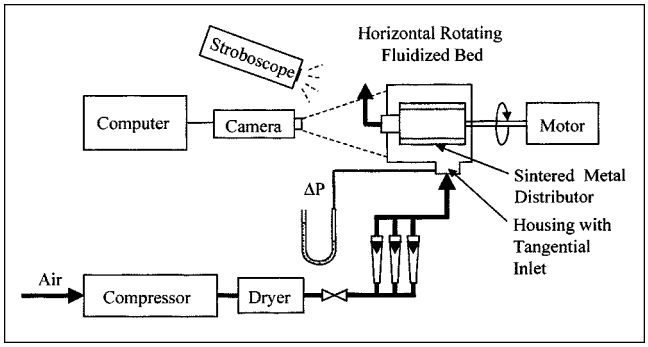

Figure 1. Experimental system.

Experimental Studies

Experimental system

The experimental system is shown in Figure 1. Dry compressed air was fed to the RFB through a bank of calibrated rotameters. A variable-speed motor provided rotating speeds between 0 to 5,000 rpm. A Pulnix progressive scan CCD Camera (Model Number: TM-1001-477; resolution: 768(H)× 494(V); shutter speed from 1/60 to 1/10,000 s) was used to study particle mixing in the RFB as a function of increasing gas velocity. The camera was connected to a computer in order to view and store the photographs in real time. All optical measurements using the Pulnix digital camera were taken perpendicularly through the Plexiglas end-plate. However, the inner surface of the rotating fluidized bed was also observed at an angle by eye and exhibited the same behavior that was seen in the photographs. Photographs showing the bed surface at an angle can also be found in our previous article (Qian et al., 1998). No accumulation of particles sticking to the Plexiglas end-plates was seen in any of our experiments, indicating that electrostatic forces for our relatively large particles were negligible.

The metal distributor (manufactured by Pall Corporation) was composed of sintered 316 low-carbon stainless steel powder with an average pore size of 55 μm and was 144 mm long. The inner radius of the distributor, which is the same as the outer radius of the bed, was 61.5 mm. To determine the inner radius of the bed precisely is difficult. The inner radius varies with the mass of particles loaded into the bed. Upon rotating the RFB, the inner surface appeared nonuniform both radially and axially in the packed-bed mode. When a

Table 1. Four Combinations of Geldart A Particles and Their Properties*

Outer Layer	Inner Layer: Alumina, White	Inner Layer: Glass, Blue	Inner Layer: Glass, White	Particle Density (kg/m^3)	Mean Dia. (by Vol.) (μm)
Alumina, black	5.4, 5.8			1,550	88.9
Alumina, white		5.0, 6.3		1,550	88.9
Glass, blue	4.8, 4.6		4.0, 4.2	2,200	84.0
Glass, white				2,200	91.3

*Ordered pairs in table give outer and inner layer thickness (mm) in that order as measured at the end-plate.

second layer of particles was added to the bed, this nonuniformity remained. At the inner surface minimum fluidization velocity (U_{mfi}) (m/s), pronounced irregularities in the bed surface disappeared, causing the surface to become more uniform. Since we used shallow beds, very little bed expansion occurs. Consequently, we have measured the thickness of both layers in the bed at U_{mfi}. These values are given in Table 1.

The rotating speed of the RFB was set at 525 rpm (55 rad/s), which is equivalent to a centrifugal acceleration of 19 times that due to gravity. The bed is initially loaded with particles of one color, and then rotated at low speed. The other colored particles are blown into the bed using a flexible tube, so that two different layers of particles are formed in the bed. The interface between the two layers is distinct and clearly visible. The bed rotational speed was then increased to 525 rpm as determined with a stroboscope. The strobe frequency was set to match the rotational frequency of the bed so that any macroscopic bubbles present could be observed. The pressure drop as a function of gas velocity and rotating speed was measured using a U-tube water manometer. Before loading particles into the bed, the pressure drop of the distributor of the empty bed was also measured.

Particle size and density

Our experiments were conducted with four combinations of Geldart-A particles as described in Table 1. The bed material consisted of blue or white glass beads provided by MO-SCI Corporation and alumina provided by the ALCOA Technical Center. The color of fresh alumina is white. Black alumina was made by coating the fresh alumina with submicron soot from a diesel engine exhaust. The effect of the soot coating on the particle-size distribution and density of the alumina was negligible. Separate experiments were performed to ascertain whether the black alumina particles have significantly different fluidization properties from the fresh white alumina particles. The pressure drop was measured as a function of gas-flow rate using a smaller 5.7 cm ID, 7.6 cm long rotating fluidized bed at two different rotating speeds. The results show that the values of the pressure drop for both materials are identical at a rotating speed of 600 rpm and are acceptably close (within experimental error) at a rotating speed of 1,000 rpm where the gas-flow rate is much higher. Thus, the very fine soot layer on the black alumina does not influence its fluidization properties.

The particle density of the glass beads is 2,200 kg/m^3, and the particle density of the alumina is 1,550 kg/m^3 (see Table 1). The particle-size distribution for all of these particles was measured using an Aerosizer (Amherst Process Instruments, Inc.), and is shown in Figure 2. The alumina particles have a relatively broad size distribution, whereas the glass beads have a much narrower size distribution. The volume average diameter size of the white glass beads, blue glass beads, and alumina are 91.3 μm, 84.0 μm, and 88.9 μm, respectively. All of them belong to group A of Geldart's powder classification based on conventional gravity-driven fluidized beds (Geldart, 1986).

Theory

The sintered metal distributor allows the fluidizing gas to flow uniformly into the bed. As the gas velocity increases, the bed changes from a packed bed to a partially fluidized bed with fluidization occurring radially outward starting at the inner surface at velocity U_{mfi}. With increasing velocity, the entire bed is fluidized at velocity U_{mfc} (m/s). Fluidization occurs in this manner because both the gas velocity (and thus the drag force) and the centrifugal force are a function of radial position in the bed. At the inner surface, the drag force is highest and the centrifugal force is lowest. The pressure drop across the bed increases linearly in the packed-bed region and becomes constant after U_{mfc} is reached, when the bed is totally fluidized. Typical curves of pressure drop through the bed vs. gas velocity for the RFB have been reported previously (Qian et al., 1998).

Uniform bed of particles

Kao et al. (1987) simplified the model of Chen (1987) for calculating the inner surface minimum fluidization velocity, the critical minimum fluidization velocity, and average minimum fluidization velocity based on the pressure drop equations for the packed and fluidized-bed regimes. In the equations given in Kao et al. (1987), the correlations suggested by Wen and Yu (1966), were used for particles of unknown

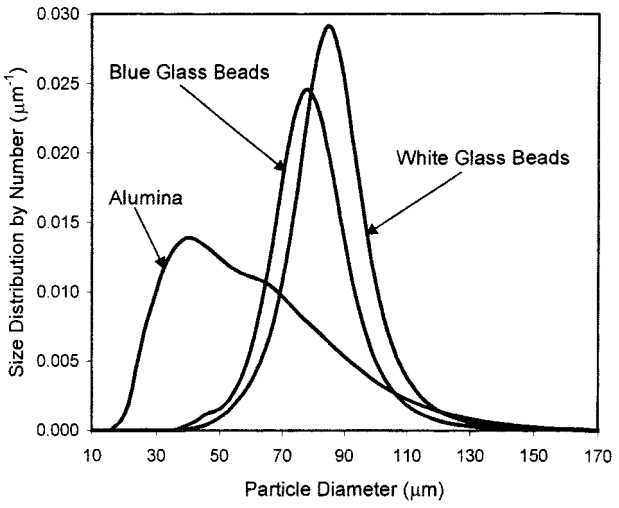

Figure 2. Particle-size distribution by number for bed materials used.

sphericity. In this article the sphericity ϕ_s (dimensionless) is taken to be unity for both the spherical glass beads and the alumina particles.

The minimum fluidization velocity at a given value of the radius r in the rotating fluidized bed based on Kao et al. (1987) is given by

$$U_{mfr} = \frac{-\phi_1 + \left[\phi_1^2 + 4\phi_2(\rho_p - \rho_g)(1-\epsilon)\omega^2 r\right]^{0.5}}{2\left(\frac{r_0}{r}\right)\phi_2} \quad (1)$$

The inner surface minimum fluidization velocity U_{mfi} (the velocity at which the inner surface of the bed is first fluidized) is obtained by letting $r = r_i$ in Eq. 1. Similarly, the critical minimum fluidization velocity U_{mfc} (the velocity at which the entire bed is fluidized) is obtained by letting $r = r_0$ in Eq. 1.

The pressure drop across the bed is a function of gas-flow rate and can be calculated from one of the following three equations:

(1) When $U_g \le U_{mfi}$, the superficial gas velocity is less than the surface minimum fluidization velocity and the bed is packed

$$\Delta P = \phi_1 U_g r_0 \ln\left(\frac{r_0}{r_i}\right) + \phi_2 U_g^2 r_0^2 \left(\frac{1}{r_i} - \frac{1}{r_0}\right) \quad (2)$$

(2) When $U_{mfi} < U_g < U_{mfc}$, the bed is partially fluidized and the pressure drop is the sum of the pressure drop across the fluidized and packed bed regions

$$\Delta P = (1-\epsilon)(\rho_p - \rho_g)\omega^2 \frac{\left(r_{pf}^2 - r_i^2\right)}{2} + \phi_1 U_g r_0 \ln\left(\frac{r_0}{r_{pf}}\right) + \phi_2 U_g^2 r_0^2 \left(\frac{1}{r_{pf}} - \frac{1}{r_0}\right) \quad (3)$$

(3) When $U_{mfc} \le U_g$, the superficial gas velocity is equal to or exceeds the critical fluidization velocity, the bed is totally fluidized and the pressure drop is

$$\Delta P = (1-\epsilon)(\rho_p - \rho_g)\omega^2 \frac{\left(r_0^2 - r_i^2\right)}{2} \quad (4)$$

Two layers of distinguishable particles

Equations for the minimum fluidization velocities and pressure drop can be derived for each of the two distinguishable layers of particles in the bed. The two layers of particles may have different minimum fluidization velocities since the density and particle-size distributions may be different. If layer 1 is next to the distributor and layer 2 is on the inside of the bed, and the radius of the interface is r_m, Eqs. 1 to 4 can be applied to each layer.

For layer 2, the inner surface minimum fluidization velocity is given by Eq. 1 with $r = r_i$ and the critical minimum fluidization velocity for that layer with $r = r_m$. Similarly, for layer 1 at the distributor, the inner surface minimum fluidization velocity is obtained from Eq. 1 with $r = r_m$ and the critical minimum fluidization velocity would be determined with $r = r_0$.

The bed pressure drop can be calculated from

$$\Delta P = \int_{r_i}^{r_m} \left(\frac{dp}{dr}\right)\Big|_{\text{layer 2}} dr + \int_{r_m}^{r_0} \left(\frac{dp}{dr}\right)\Big|_{\text{layer 1}} dr \quad (5)$$

where the pressure drop in each layer is determined from Eqs. 2–4.

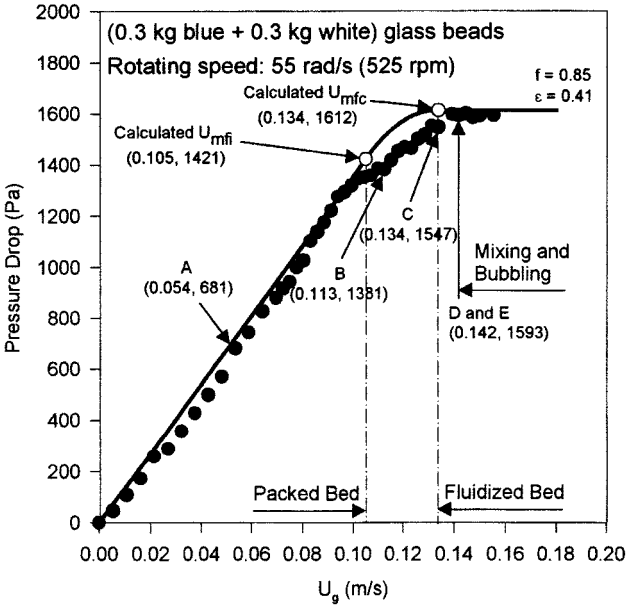

Figure 3. Pressure drop as a function of superficial gas velocity for two different colored layers of glass beads.

A to E refer to the photographs in Figure 4.

Results and Discussion

The experimental results are presented for the four different particle systems investigated.

Blue and white glass beads

Blue glass beads (0.3 kg) were placed on the distributor and the RFB was rotated. As the bed was rotating, white glass beads (0.3 kg) were added to the bed to produce two distinguishable layers of particles. The interface between the two colored layers is distinct and clearly visible. However, the radial location of the inner surface of the white beads is generally not uniform due to the method used to introduce the second layer. As the gas velocity was increased, the pressure drop of the bed was measured. Figure 3 shows the measured points of net pressure drop (total pressure drop less the pressure drop of the distributor) as a function of gas velocity. Figure 3 also shows the theoretical pressure drop curve with the theoretically calculated inner surface and critical minimum fluidization velocities. In order to fit the experimental data to the theoretical curves, the weight of the particles was multiplied by a correction factor f equal to 0.85.

The application of this factor is reasonable for the following reasons. First, a large number of experiments were conducted in the RFB where particles were weighed before and after the experimental run. Data from 12 different runs using either alumina or glass beads as the bed material showed an average weight loss of the order of 5% of the bed weight. Some particles were lost during the initial fill-in procedure, some were lost due to elutriation at high gas velocities, and still others were lost whenever the bed rotation was started or stopped. However, the major contribution to the correction factor f is due to the nonuniformity of the bed thickness both radially and axially. The effect of gravity alone produces a somewhat thicker bed at the bottom compared to the top of the horizontal rotating bed. For example, at 525 rpm, the centrifugal acceleration is about 19 g. The resulting difference of approximately 5% in the radial thickness of the bed allows more gas to percolate through the thinner part of the bed giving a lower pressure drop than predicted by theory. This phenomenon was pointed out by Chen (1987), who compared the experimental data of the pressure drop in a rotating fluidized bed obtained by many different investigators (Fan et al., 1985; Demircan et al., 1978; Levy et al., 1978) to the theory. Chen concluded that the theory always overpredicts the data with an average error of more than 10% and sometimes as much as 20%. Thus, setting $f = 0.85$ for the glass beads is consistent with our experimental observations, as well as with previous experimental data.

By assuming a constant voidage of 0.41, the theoretical and experimental values of U_{mfi} and U_{mfc} in Figure 3 are seen to be in excellent agreement. However, it should be noted that in a rotating fluidized bed, as opposed to a conventional fluidized bed, there can be small radial variations in bed voidage due to differences in local velocities and centrifugal acceleration (Mutsers and Rietema, 1977; Chen, 1987).

When $U_g < 0.105$ m/s, the predicted value of U_{mfi}, the RFB is expected to be in the packed-bed regime. Several photographs were taken in this range. Figure 4A ($U_g = 0.054$ m/s) shows a typical photograph of the bed. The bed had a nonuniform surface due to the method of filling the second layer of particles with different color, as discussed above. In this condition, the particles are static relative to each other and behave as a solid.

As the gas velocity was increased to $U_g = 0.113$ m/s, the bed surface started to become more uniform, as shown in Figure 4B. Particles begin to fluidize at U_{mfi}. Upon increasing the gas velocity further the bed begins to fluidize outwardly until the entire bed is fluidized at U_{mfc}. Between the inner surface and the critical minimum fluidization velocities, the bed is partially fluidized. In this range, particles are still relatively stable in relation to one another. The two different colored layers of particles have not mixed yet, indicating that particles have not moved in the radial direction. However, those particles that have already been fluidized close to the inner surface of the bed appear to have moved along the surface and the bed has become somewhat fluid-like. As the gas velocity is increased further, the bed surface became more uniform, that is, the inner surface of the white glass beads is sharply delineated, as can be seen in Figure 4C at $U_g = 0.134$ m/s.

In theory, the minimum gas velocity at which the first inner layer of particles can begin to move is the inner surface minimum fluidization velocity U_{mfi}. The surface should start to become more uniform at this point. However, detecting this onset is difficult using either a camera or through visual observation. It is noted that the inner surface velocity is slightly lower than 0.113 m/s (Figure 4B), but higher than 0.102 m/s at which a photograph (not shown) indicated that the bed was still packed. Our theoretical calculation indicates that the inner surface gas velocity (U_{mfi}) is 0.105 m/s and the critical fluidization velocity (U_{mfc}) is 0.134 m/s.

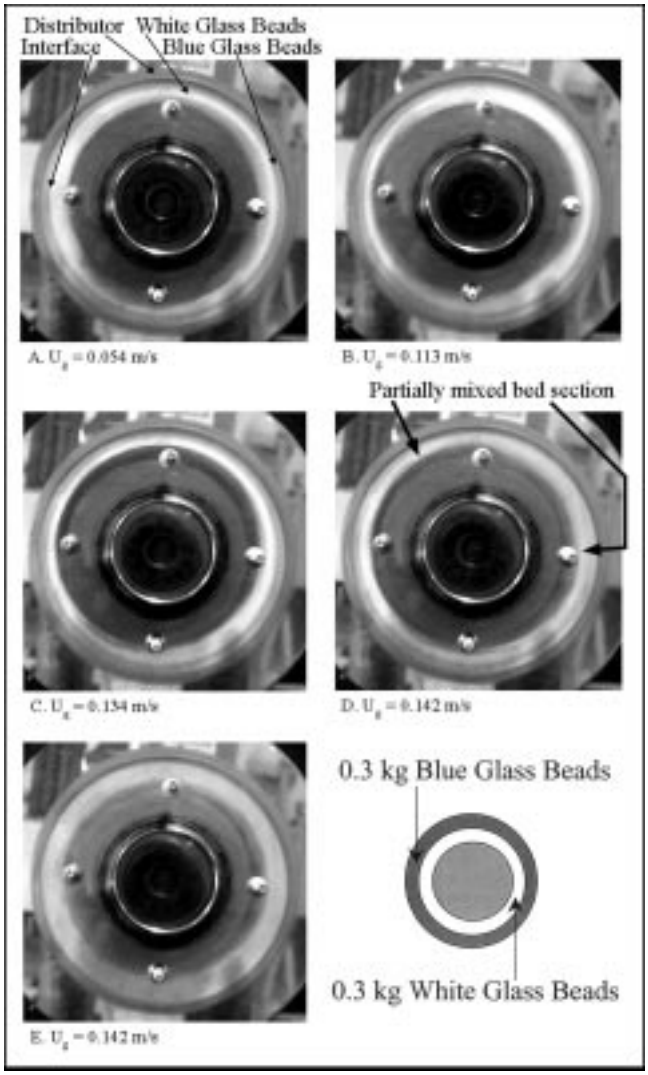

Figure 4. RFB at different superficial gas velocities for blue and white glass beads.

When $U_g = 0.142$ m/s, the particles began to mix and the interface between the two colored layers became diffuse. Figure 4D shows that the particles are partially mixed. The interface between the two colored layers disappears in the bed section between the two arrows in the figure. This condition was frozen by quickly lowering the gas-flow rate. The photograph was taken and then $U_g = 0.142$ m/s was reset. The entire bed became mixed very rapidly. There is no visible interface, as shown in Figure 4E. The gas velocity at which the bed became totally mixed was slightly higher than the theoretical U_{mfc}, as would be expected for Geldart-A parti-

cles. However, this slight difference is within experimental error and does not clearly indicate a nonbubbling totally fluidized-bed regime before mixing occurs. Bubbles were also observed when the mixing velocity was reestablished. This observation indicates that bubbles cause the bulk motion of the particles in the radial direction, in agreement with the results of Menon and Durian (1997). In contrast to their results, there is no clearly discernible difference between U_{mfc} and the minimum bubbling velocity U_{mb}, that is, they either coincide or are nearly equal.

For gas velocities between U_{mfr} for $r = r_m$ (the radius of the interface) and U_{mfc}, the interface between the two colored layers is in the fluidized region of the bed. At velocities in this interval, particle motion and mixing of the two layers could occur by particle diffusion. However, during the time when U_g was greater than U_{mfi} and less than U_{mb}, and, thus, could have been in this interval, no "blurring" of the interface was observed either visually or upon examination of the digital photographs. Mixing due to diffusion occurs on a much longer time scale than the rapid mixing observed at the onset of bubbling. Thus, to the extent that particle motion occurred at the interface due to diffusion, it did so on a length scale too small to be observed in our experiments.

Particle motion and mixing can also occur due to circulation flow in a fluidized bed. However, our beds are very thin compared to conventional fluidized beds. Consider, for example, the ratio of the area of the bed in contact with the wall (end-plates for the RFB) to the area of the bed perpendicular to the gas flow at the distributor. In our beds, that ratio is on the order of 0.1 compared to the value of 4 for a conventional bed of circular cross-section and height equal to one diameter. Thus, a significant effect due to shear at the wall would not be expected. Indeed, no circulation flow was observed in our experiments.

Black alumina and white alumina

In order to verify the above results, alumina was used instead of glass beads in the same experiment. The average particle size of the alumina is almost the same as that of the glass beads, but its density is lower and its size distribution is much wider. The alumina particles, like the glass beads, fall into the Geldart-A classification for conventional fluidized beds. Black alumina (0.4 kg) was filled into the bed and, while the RFB was rotating, white alumina (0.3 kg) was loaded into the bed. Figure 5 presents the experimental pressure drop values and the theoretically calculated curve (less pressure drop of the distributor) as a function of gas velocity. The bed voidage used was 0.425. The measured weight of the alumina was multiplied by a correction factor (dimensionless) $f = 0.80$ in order to fit the experimental points to the theoretical curve for the same reasons as given above for the glass beads. The small difference in f factors for the glass beads and alumina particles is probably due to the fact that the alumina particles have a much wider size distribution with more smaller particles (see Figure 2).

The experimental method was the same as was used for the glass beads. When $U_g < 0.074$ m/s, the predicted U_{mfi}, the RFB is in the packed-bed regime. In this condition, the bed surface is not uniform due to the fill-in procedure and particles in the two layers did not mix. Several photographs

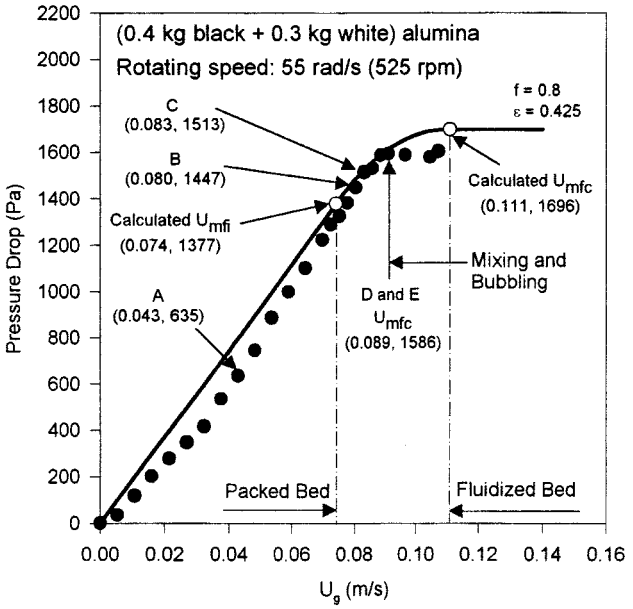

Figure 5. Pressure drop as a function of superficial gas velocity for two different colored layers of alumina.

A to E refer to the photographs in Figure 6.

were taken. These photographs all show the same structure of the bed, as illustrated in Figure 6A ($U_g = 0.043$ m/s).

The first change was observed at 0.080 m/s (Figure 6B). The bed surface started to become uniform. Between U_{mfi} and U_{mfc}, the bed was partially fluidized. However, the black and the white particles did not mix. Figure 6C shows a photograph of the bed at $U_g = 0.083$ m/s. Mixing had not occurred, but the inner surface of the bed had become even more uniform than in Figure 6B.

Figure 6D shows a photograph that was taken at $U_g = 0.089$ m/s, when the bed was partially mixed. Again, the interface between the two colored layers disappears in the bed section between the two arrows in the figure. This condition was frozen by lowering the gas-flow rate. After the photograph was taken, the same gas velocity was reset. A couple of seconds later, total mixing of the bed occurred, and bubbles appeared as shown in Figure 6E. Based on the pressure drop curve and this observation, the experimental U_{mfc} is estimated to be 0.089 m/s. It is the first point at which the gas velocity has no effect on pressure drop, that is, the pressure drop becomes constant. The theoretical calculation gave a higher $U_{mfc} = 0.111$ m/s. Even though these particles are in the Geldart-A classification, the mixing point appears to occur at the experimentally measured U_{mfc}, which, within observational uncertainty, is also the minimum bubbling velocity. Again, before bubbling, neither small-scale mixing at the interface nor establishment of circulation flow were observed.

Blue glass beads outside and white alumina inside

Since the densities and size distribution of the alumina particles and glass beads are different, their minimum fluidization velocities are also different. In order to investigate

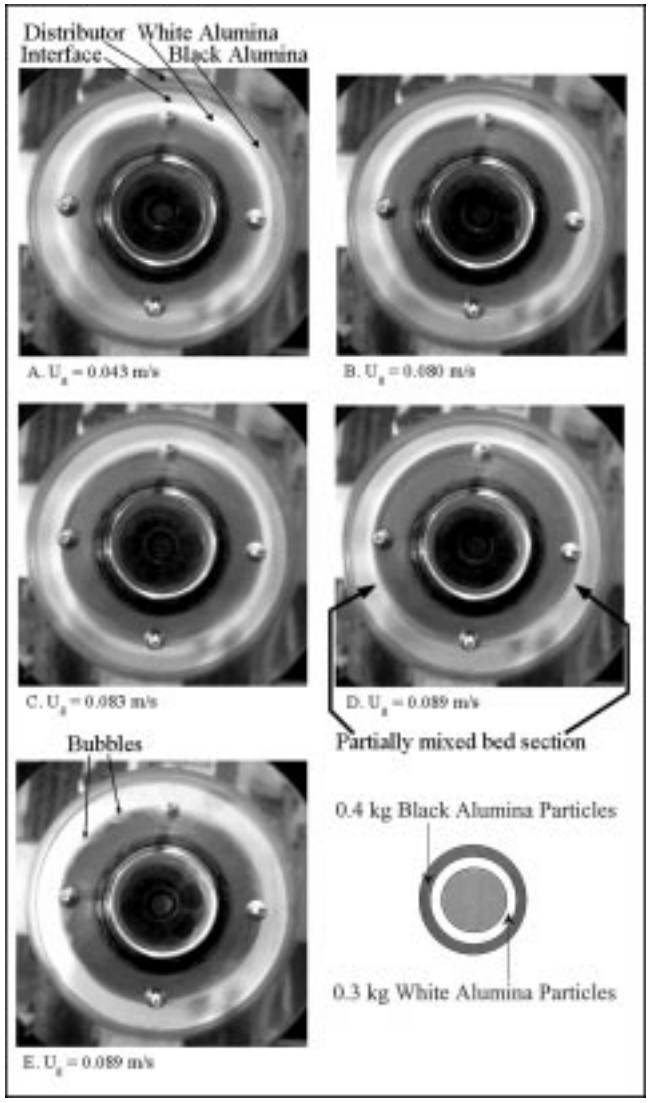

Figure 6. RFB at different superficial gas velocities for black and white alumina.

the mixing properties for particles of different materials having different densities, blue glass beads (0.4 kg) were loaded into the bed first. While the RFB was rotating, white alumina (0.3 kg) was filled into the bed giving two layers of particles with different colors and densities. Again, the pressure drop of the bed was measured as the gas velocity was increased. Figure 7 shows the experimentally measured pressure drop points and the theoretically calculated curve vs. gas velocity. The previously used voidages and correction factors for the glass beads and the alumina were used in calculating the pressure drop curve. Figure 8 shows the photographs that were taken during this experiment.

Until point A ($U_g = 0.080$ m/s) in Figure 7, the inner bed surface was nonuniform, as can be observed in Figure 8A. The next measurement point was at $U_g = 0.086$ m/s. As the alumina inner surface began to fluidize, the surface became more uniform very quickly, as shown in Figure 8B. The calculated minimum fluidization velocities are as follows: for the layer of glass beads, $U_{mfi} = 0.105$ m/s and $U_{mfc} = 0.122$ m/s;

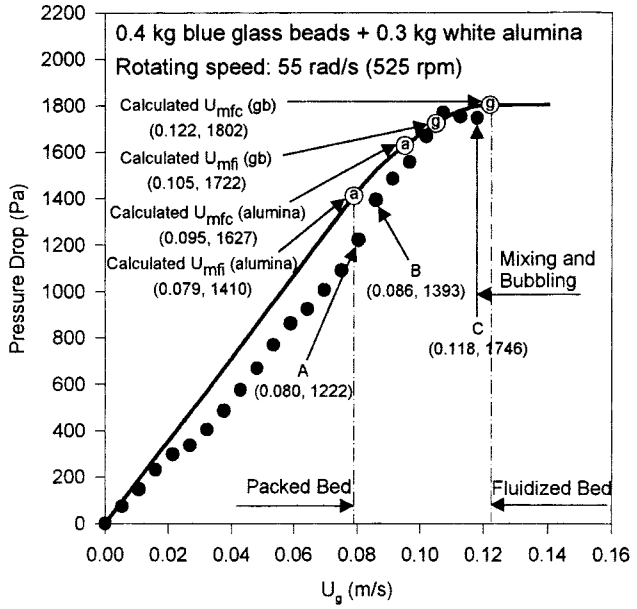

Figure 7. Pressure drop as a function of superficial gas velocity for blue glass beads and white alumina layers.

A to C refer to the photographs in Figure 8.

for the layer of alumina, $U_{mfi} = 0.079$ m/s and $U_{mfc} = 0.095$ m/s. It is believed that the photograph at point A was taken just before the inner surface minimum fluidization velocity was reached, although the velocity at this point is approxi-

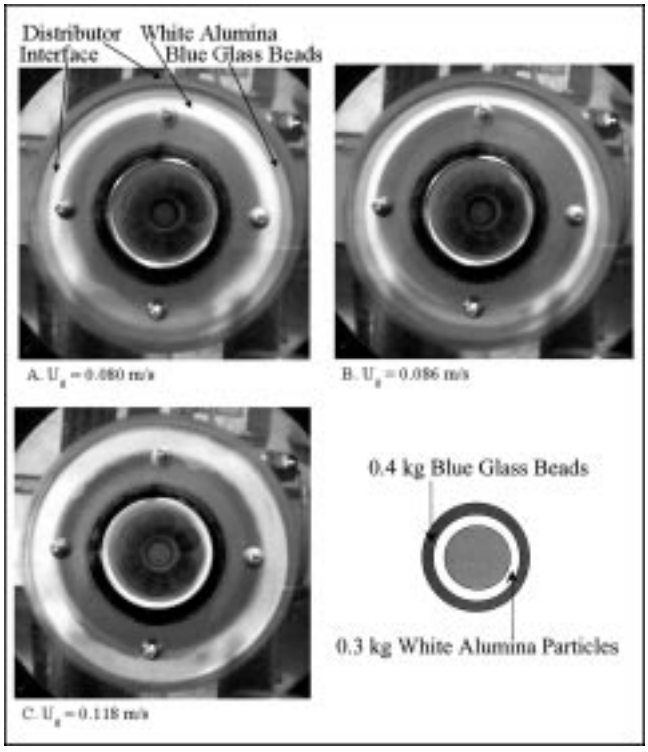

Figure 8. RFB at different superficial gas velocities for blue glass beads and white alumina powder.

mately equal to the calculated U_{mfi} for the alumina. It appears that the entire layer of alumina began to fluidize before the glass beads started to fluidize. Photographs could not be taken showing the surface becoming progressively more uniform. However, it was observed that a thin light blue layer intermediate between the darker blue glass beads inner layer and the white alumina outer layer formed when the glass beads began to fluidize. This thin layer did not grow and was seen until total mixing of the bed was obtained with bubbles appearing, as shown in Figure 8C at $U_g = 0.118$ m/s. At this point, the particles mixed very quickly.

The observed behavior can be explained by the fact that the alumina particles were already totally fluidized by the time the entire glass bead layer became fluidized. Therefore, the mixing was very fast. The particles mixed when the glass beads reached the critical fluidization velocity. It appears, however, that the theoretical calculations give higher values of the minimum fluidization velocities than those observed experimentally.

White alumina outside and blue glass beads inside

Alumina particles (0.3 kg) having a lower density than the glass beads were placed on the outside of the bed adjacent to the distributor. Glass beads (0.5 kg) were filled on the inside of the bed. In this case the mixing behavior was entirely different from that observed in the previous experiments. As the gas velocity was increased, the bed pressure drop was measured. Figure 9 presents the experimental pressure drop points and the theoretically calculated curve as a function of gas velocity. The calculation method and the correction factors were the same as had been used previously. As can be seen from the figure, in this case the theoretical pressure drop curve overpredicts the experimental values in both the packed and fluidized-bed regimes. Figure 10 shows the photographs that were taken during the experiment.

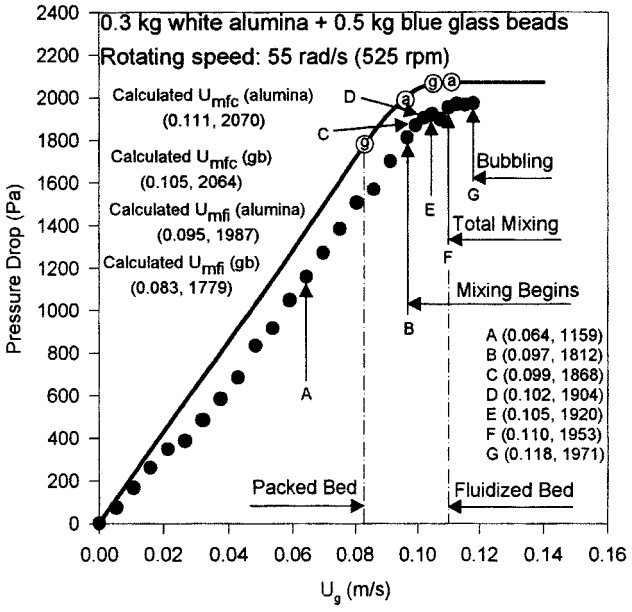

Figure 9. Pressure drop as a function of superficial gas velocity for white alumina and blue glass beads layers.

A to G refer to the photographs in Figure 10.

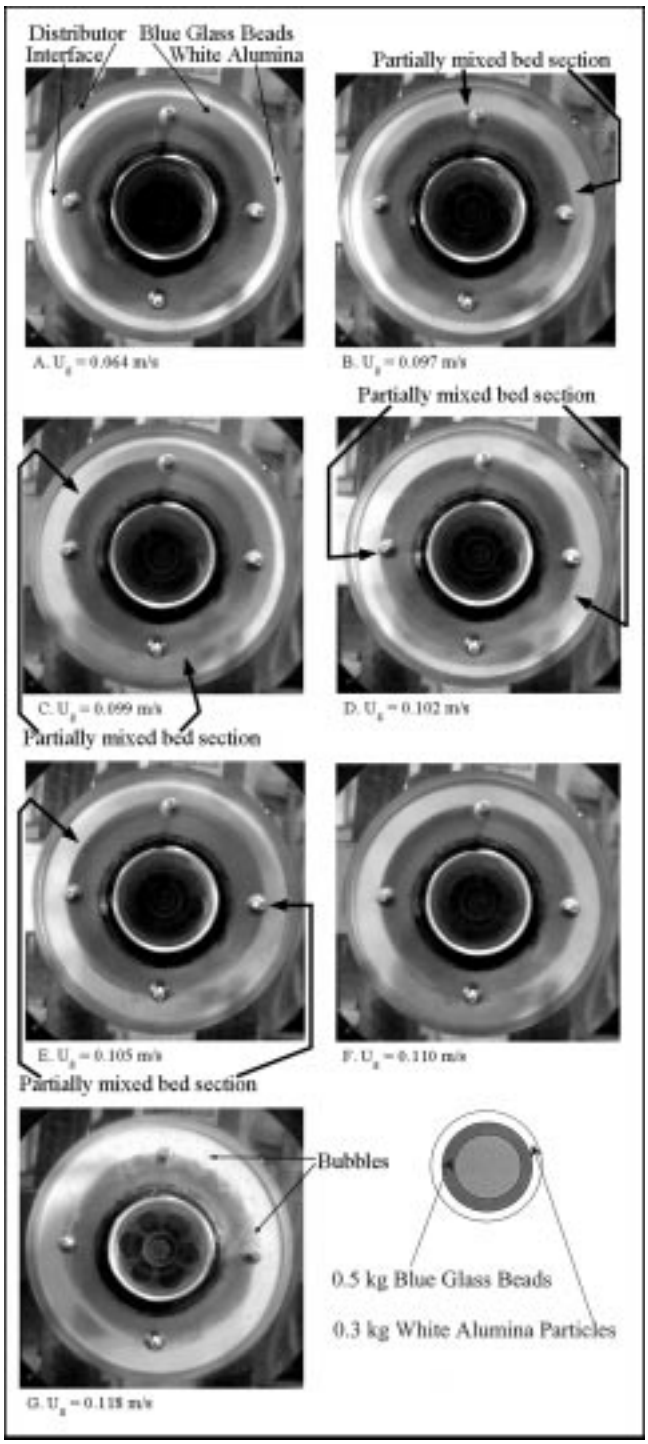

Figure 10. RFB at different superficial gas velocities for white alumina and blue glass beads.

At point A ($U_g = 0.064$ m/s) in Figure 9, neither the glass beads nor the alumina are fluidized, that is, both layers are in the packed-bed regime. The particles were stationary relative to each other and, therefore, the inner surface of the bed was not uniform, as shown in Figure 10A. In the packed bed

regime several photographs were taken without any changes in the appearance of the bed surface.

At $U_g = 0.097$ m/s, the bed surface became more uniform. At the same time, a radial segment of the bed began to mix without observing any bubbles as shown in Figure 10B. The appearance of the more uniform surface occurred very quickly. At the previous measurement point ($U_g = 0.091$ m/s, not shown), the bed surface was still not uniform even though the glass beads may have become fluidized based on the theoretical pressure drop curves. The next three photographs (Figures 10C, 10D, and 10E) show that the mixed region (between the two arrows where the interface is no longer visible) grew larger as the gas velocity was increased. Eventually, at 0.110 m/s the entire bed became mixed (no interface) as can be seen in Figure 10F. Bubbles were not observed at this gas velocity. Bubbles appeared later at 0.118 m/s.

The calculated fluidization velocities for the layers of glass beads and alumina are: $U_{mfi} = 0.083$ m/s and $U_{mfc} = 0.105$ m/s, and $U_{mfi} = 0.095$ m/s, and $U_{mfc} = 0.111$ m/s, respectively. Thus, the glass beads had already been partially fluidized when the alumina particles started to become fluidized at 0.095 m/s. However, the outer portion of the inner layer of glass beads remained in the packed-bed regime. This packed bed layer covered the alumina particles as a ''lid'' preventing the expansion of the particles in the alumina layer. Once all of the glass beads became fluidized, the ''lid'' was removed, and the entire bed proceeded to fluidize.

Unlike the previous experiments, the mixing of the bed began at the gas velocity at which the alumina particles started to become fluidized. At this point, a small section of the bed started to mix (see Figure 10B) and grow (see Figures 10C, 10D, and 10E) until the entire bed was fluidized (see Figure 10F). In contrast to the virtually instantaneous mixing observed in the prior experiments, density driven mixing occurs gradually because the more dense glass beads move into the fluidized alumina layer due to the centrifugal force. Bubbles were not observed until $U_g = 0.118$ m/s, which was somewhat higher than the velocity of total mixing (see Figure 10G).

Conclusions

For particles of the same material, the two layers of particles do not mix until bubbles appear. This result is similar to that of Menon and Durian (1997), who concluded that bubbles are responsible for the bulk motion of particles in the conventional fluidized bed used in their study. Below U_{mfi}, the bed behaves as a solid. Between the calculated U_{mfi} and U_{mfc}, the inner surface is observed to become more uniform, that is, in this respect, the bed exhibits fluid-like behavior before mixing. After U_{mfc}, particles inside the bed start to move radially and mixing occurs rapidly. Bubbles are a strong source of particle motion, and the bed becomes totally fluid-like. To within observational error, mixing and the occurrence of minimum critical fluidization velocity and minimum bubbling velocity coincide. These results are different from these of Menon and Durian (1997) who found bubbling to occur in their gravity-driven bed at a velocity appreciably greater than the minimum fluidization velocity for Geldart-A particles. Figure 11 shows these ideas.

For conventional fluidized beds, the minimum bubbling velocity U_{mb} is dependent on the size and density of the particles. For Geldart-B particles, U_{mb} is equal to the minimum fluidization velocity U_{mf}, whereas for Geldart-A particles, which were used in our experiments, U_{mb} is larger than U_{mf} so that there is an appreciable operating region in which the bed is fluidized, but not yet bubbling. Cody et al. (1998) suggest that particle circulation in a conventional circular cross-section fluidized bed, which leads to shear forces, may be responsible for Geldart-A behavior. Our RFB has negligible wall effects and, hence, presumably negligible particle circulation. The fact that no mixing of particles occurs before bubbles are observed could be a consequence of the hypothesis of Cody et al. that Geldart-A fluidization is dependent on circulation within the fluidized bed and can mimic Geldart-B like behavior when particle circulation is absent. On the other hand, an RFB differs from a conventional fluidized bed in that the acceleration field is considerably greater than gravity. Therefore, previous studies in conventional fluidized beds to determine U_{mb} may not be relevant. Indeed, the location of the Geldart A/B boundary in the diameter-density plane is likely to be a function of the magnitude of the effective acceleration field. Our results are also consistent with the hypothesis that a shift in the location of this boundary occurs that results in particles in the Geldart-A classification for conventional beds exhibiting Geldart-B behavior in an RFB. A theoretical analysis of this issue will be presented in the future.

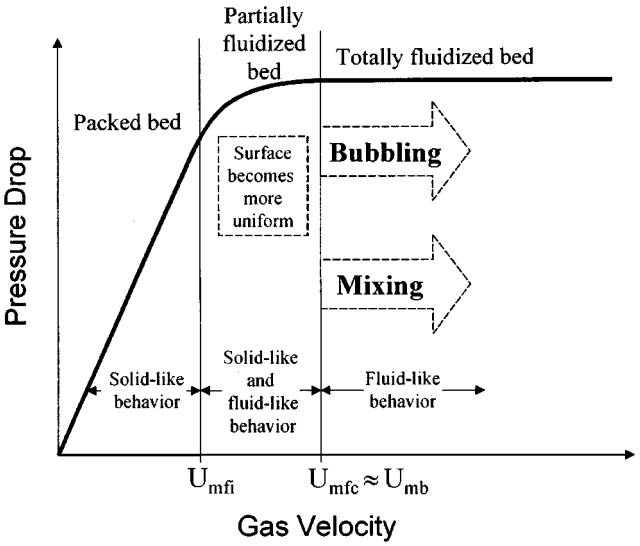

Figure 11. Operating region.

For particles of different density, the mixing characteristics of the two layers depend on whether or not the denser particles are near the distributor. When the denser particles are near the distributor, the mixing behavior is very similar to that of particles of the same density. When the less dense particles are near the distributor, the mixing behavior is quite different. Mixing occurs gradually due to the differences in density and fluidization properties of the two layers, and total mixing is observed before bubbles appear.

Acknowledgments

This research was supported by the National Science Foundation under grant No. CTS-9612483 and the EPA Exploratory Research

Center on Airborne Organics under grant No. R824970. We would like to express our appreciation to Ian W. Burdick for his assistance in preparing this article and enhancing the photographs.

Notation

d_p = particle diameter, m
r_0 = distributor radius, m
r_i = inner surface radius, m
r_m = radius of interface between the two layers of particles, m
r_{pf} = radius of interface of fluidized and packed beds, m
U_g = superficial gas velocity based on outside radius r_0, m/s
U_{mb} = minimum bubbling velocity, m/s
U_{mfc} = critical minimum fluidization velocity, m/s
U_{mfi} = inner surface minimum fluidization velocity, m/s
U_{mfr} = minimum fluidization velocity at a given value of radius (r) in the RFB, m/s
ΔP = pressure drop across the bed, Pa
ϵ = voidage, dimensionless
μ = viscosity, kg/m·s
ρ_g = gas density, kg/m^3
ρ_p = particle density, kg/m^3
ϕ_1 = coefficient in Ergun equation, $\phi_1 = [150(1-\epsilon)^2\mu]/\epsilon^3(\phi_s d_p)^2$, kg/m^3·s
ϕ_2 = coefficient in Ergun equation, $\phi_2 = [1.75(1-\epsilon)\rho_g]/\epsilon^3\phi_s d_p$, kg/m^4
ω = rotating speed, rad/s

Literature Cited

Buyevich, Y. A., "Fluid Dynamics of Coarse Dispersion," *Chem. Eng. Sci.*, **49**, 1217 (1994).

Buyevich, Y. A., and S. K. Kapbasov, "Polydisperse Fluidization: 1. Basic Equation," *Chem. Eng. Sci.*, **49**, 1245 (1994).

Chen, Y., "Fundamentals of a Centrifugal Fluidized Bed," *AIChE J.*, **33**, 722 (1987).

Cody, G. D., and D. J. Goldfarb, "Discontinuity in Particle Granular Temperature of Across the Geldart B/A Boundary," *Prog. in Fluidization and Fluid Particle Systems*, AIChE Symp. Series, D. King, ed., **93**, 18 (1997).

Cody, G. D., D. J. Goldfarb, G. V. Storch, Jr., and A. N. Norris, "Particle Granular Temperature in Gas Fluidized Beds," *Powder Technol.*, **87**, 211 (1996).

Cody, G. D., S. K. Kapbasov, and Y. A. Buyevich, "Particle Fluctuation Velocity in Gas Fluidized Beds—Fundamental Models Compared to Recent Experimental Data," Symp. B, Adv. Technol. in Fluid-Particle System, AIChE Meeting, Miami Beach (1998).

Davidson, J. F., R. Clift, and D. Harrison, *Fluidization*, Academic Press, London (1985).

Demircan, N., B. H. Gibbs, J. Swithenbank, and D. S. Taylor, "Rotating Fluidized Bed Combustor," *Fluidization*, J. F. Davidson and D. L. Kearins, eds., Cambridge University Press, Cambridge, p. 270 (1978).

Fan, L. T., C. C. Chang, Y. S. Yu, T. Takahashi, and Z. Tanaka, "Incipient Fluidization Condition for a Centrifugal Fluidized Bed," *AIChE J.*, **31**, 999 (1985).

Geldart, D., *Gas Fluidization Technology*, Wiley, New York (1986).

Jackson, R., "The Nature and Role of Effective Stress in Fluidized Systems," *Fluidization IX*, L. S. Fan and T. M. Knowlton, eds., Engineering Foundation, New York (1998).

Kao, J., R. Pfeffer, and G. I. Tardos, "On Partial Fluidization in Rotating Fluidized Beds," *AIChE J.*, **33**, 858 (1987).

Kroger, D. G., G. Abdelnour, E. K. Levy, and J. C. Chen, "Particle Distribution and Mixing in a Centrifugal Fluidized Bed," *Fluidization*, J. R. Grace and J. M. Matsen, ed., Plenum Press, New York, p. 453 (1980).

Levy, E. K., W. J. Shakespeare, A. Tabatabaie-Raissi, and J. C. Chen, "Particle Elutriation from Centrifugal Fluidized Beds," *Recent Advances in Fluidization*, AIChE Symp. Ser., **77**(205), 86 (1981).

Levy, E. N., N. Martin, and J. Chen, "Minimum Fluidization and Startup of a Centrifugal Fluidized Bed," *Fluidization*, D. L. Kearins, ed., Cambridge University Press, Cambridge (1978).

Menon, N., and D. J. Durian, "Particle Motions in a Gas-Fluidized Bed of Sand," *Phys. Rev. Lett.*, **79**, 3407 (1997).

Mutsers, S. M. P., and K. Rietema, "Gas-Solids Fluidization in a Centrifugal Field: The Effect of Gravity upon Bed Expansion," *Powder Technol.*, **18**, 249 (1977).

Qian, G. H., I. Bágyi, R. Pfeffer, H. Shaw, and J. G. Stevens, "A Parametric Study of a Horizontal Rotating Fluidized Bed Using Slotted and Sintered Metal Cylindrical Gas Distributors," *Powder Technol.*, **100**, 190 (1998).

Tsinontides, S. C., and R. Jackson, "The Mechanics of Gas Fluidized Beds with an Interval of Stable Fluidization," *J. of Fluid Mechanics*, **255**, 237 (1993).

Wen, C. Y., and Y. H. Yu, "A Generalized Method for Predicting the Minimum Fluidization Velocity," *Chem. Eng. Symp. Ser.*, **67**, 100 (1966).

Manuscript received Sept. 28, 1998, and revision received Apr. 21, 1999.